Journal Pre-proof

Interactions between feed solutes and inorganic electrolytic draw solutes in forward osmosis

Arnout K.H. D'Haese

PII: S0376-7388(19)31822-8

DOI: https://doi.org/10.1016/j.memsci.2019.117636

Reference: MEMSCI 117636

To appear in: *Journal of Membrane Science*

Received Date: 18 June 2019

Revised Date: 20 September 2019

Accepted Date: 3 November 2019

Please cite this article as: A.K.H. D'Haese, Interactions between feed solutes and inorganic electrolytic draw solutes in forward osmosis, *Journal of Membrane Science* (2019), doi: https://doi.org/10.1016/j.memsci.2019.117636.

Interactions between feed solutes and inorganic electrolytic draw solutes in forward osmosis

Arnout K.H. D'Haese[a,*]

[a] *Particle and Interfacial Technology group (PaInT), Department of Applied Analytical and Physical Chemistry, Faculty of Bioscience Engineering, Ghent University, Coupure Links 653, B-9000, Ghent, Belgium*

Abstract

A comprehensive transport model for Forward Osmosis (FO) is presented, based on Maxwell-Stefan theory. In FO, the oppositely directed fluxes give rise to frictional interactions, while the salinity gradient also causes to thermodynamic non-ideal behaviour of organic feed solutes, in the form of salting out. When using electrolytic draw solutes, unequal ion permeance of the draw solute creates an electrostatic potential difference across the membrane, which is an additional driving force for transport of ionic feed solutes. A sensitivity analysis is presented, assessing the effect of frictional interactions, partitioning of feed and draw solutes and salting out on feed solute rejection. It is shown that feed solute rejection is determined primarily by friction with the membrane polymer and partitioning, and secondary by salting out. Frictional interaction between feed and draw solutes is not significant for active layer transport, for a wide range of parameter variation. It can however be significant for transport in the support layer, once feed solutes have permeated through the active layer. Electromigration can be as important as diffusively-driven transport, provided that the length over which the electrostatic potential is established is limited to about the thickness of the active layer. Finally, additional interactions between membranes, organic and inorganic solutes are discussed.

Keywords: forward osmosis, trace organic contaminants, transport modelling, Maxwell-Stefan; sensitivity analysis

1. Introduction

Forward osmosis (FO) is a dense water filtration membrane process in which water transport is driven by a salinity gradient across the membrane, in contrast to a pressure gradient used in reverse osmosis (RO) or nanofiltration (NF). This gives rise to an additional flux of the draw solute towards the feed solution, and is oppositely directed compared to water and feed solute fluxes. The high salinity of the draw solute and the additional flux cause certain interactions with the membrane and other fluxes, which are obviously not present in pressure-driven systems. These interactions include frictional hindrance between feed and draw solute fluxes, as proposed by Xie et al. [1], ion exchange [2, 3, 4, 5, 6, 7], altered solute-membrane affinity [8] and salting out. Frictional hindrance between feed and draw solute fluxes was proposed as the mechanism to explain higher rejection of organic micropollutants (OMPs) in FO compared to the same membrane

*Corresponding author
Email address: arnout.dhaese@ugent.be (Arnout K.H. D'Haese)

operated using RO [1]. However, higher OMP rejection in FO was not confirmed in a subsequent study by Kong et al. [9], and the permeance of FO membranes to OMPs was also found to be similar with or without the presence of salts [10]. Ion exchange through FO membranes seems to be mainly driven by cation exchange [3, 6, 7], and it obviously requires a significant concentration of mobile ions in both the feed and draw solutions for ion exchange to be significant [7]. It is accelerated at high pH, through the deprotonation of polyamide creating a higher anionic charge density [6]. Nitrate appears to be an anion of exceptionally high mobility as well [3, 4].

Most of the studies into these phenomena have however been experimental in nature, and a rigorous theoretical study on interactions between feed and draw solutes has so far been lacking. Moreover, to the best of the author's knowledge, no FO transport models so far have included salting out. Salting out is the increase in activity of an organic solute in the presence of mineral salts. Many different mechanisms have been proposed to explain this phenomenon, including reduced hydration of the organic solutes, electrostriction, the lower relative permittivity of organic solutes compared to water and more [11]. The propensity of a solute to salting out has been shown to be strongly correlated to its hydrophobicity [12]. The relevance of salting out for FO is of course related to the salinity gradient installed by the draw solute, which alters the chemical potential gradient across the membrane of organic feed solutes and thereby alters the driving force for organic feed solute transport. Salting out has been shown to decrease organic solute rejection in nanofiltration [13, 14, 15, 16], but in FO, it would contribute to organic feed solute rejection, because the salinity gradient is oppositely directed compared to the NF cases.

This study aims to investigate interactions between feed and draw solutes from a theoretical point of view. The appropriate framework to study both frictional interactions, kinetic in nature, as well as the thermodynamic driving forces for multicomponent membrane transport is the Maxwell-Stefan (M-S) transport model. This very general transport model originates from a force balance between thermodynamic driving forces accelerating particles of a given type on the one hand, and friction with particles of other types [17, 18]. It follows that frictional interactions are explicitly separated from thermodynamic driving forces, in contrast to Fickian diffusion. The M-S diffusivities can be considered as binary inverse friction factors between two system components, and show only weak concentration dependence, again in contrast to Fickian diffusion [18]. M-S diffusivities need to be calculated from experimental Fickian diffusivities, who can be transformed into each other by accounting for thermodynamic non-ideality factors [18]. The M-S theory has been adapted for highly dissimilar systems such as polymeric membranes transmitting small, mobile species [19, 20, 21], and M-S diffusivities can be predicted from molecular dynamics simulations as well [17, 22]. The developed model will be explained in detail in the subsequent section.

The goal of this study is to quantitatively assess the importance of different feed solute - draw solute interactions, including friction in the active layer and support layer, as well as salting out and electromigration. A novel and comprehensive FO transport model is presented, which was used to study feed solute transport. The draw solute was assumed to be NaCl throughout the study, while the feed solute was assumed to be an organic micropollutant (OMP), and is applicable to both neutral and charged solutes. The model can be extended

easily to inorganic electrolytic feed solutes as well. The sensitivity of feed solute transport through the active layer to frictional coupling, partitioning as well as salting out was investigated by means of a Sobol sensitivity analysis, in which six factors were varied over a wide range so as to include "extreme" conditions. Frictional hindrance during transport in the support layer was assessed as well. To this end, friction factors between OMPs and the draw solute were calculated and related to frictional hindrance during transport through the support layer. It is shown that frictional feed solute - draw solute interactions are not important, while salting out significantly contributes to feed solute rejection. Electromigration, the driving force for ion exchange, is shown to be a significant driving force for transport of electrolytes, provided most of the electrostatic potential gradient is localized over the active layer only.

2. Theory

2.1. Active layer transport model

A Maxwell-Stefan transport model for FO was constructed, starting from the thermodynamically rigorous formulation for solvent-polymer systems by Fornasiero et al. [19]:

$$-\frac{c_i}{RT}\nabla\mu_i = \sum_{j=1,j\neq i}^{n-1} \frac{\phi_i\phi_j(u_i - u_j)}{\bar{v}Đ_{ij}} \tag{1}$$

in which c_i, ϕ_i and u_i are the concentration, volume fraction and velocity of component i. $Đ_{ij}$ are the binary Maxwell-Stefan (M-S) diffusion coefficients, which can be considered as inverse friction factors. In contrast to Fickian diffusion coefficients, the M-S diffusion coefficients are determined by frictional interactions only, and are not influenced by solution non-ideality. This leads to a low concentration dependence of M-S diffusion coefficients [18]. Given that the molar volume of the polymer is ill-defined and starkly different compared to the solvent and solutes, volume fractions instead of mole fractions are used. All concentrations are related to volume fractions by means of $\bar{v}$, a reference molar volume, typically being the molar volume of the smallest component present in the mixture, which is water in this system. In this study, FO is described by four components: membrane, water, feed solute and draw solute, resulting in a system of three equations containing six binary diffusion coefficients. Due to Onsager's reciprocity relations, $Đ_{ij} = Đ_{ji}$. The membrane phase has an associated volume fraction ϕ_m and contributes to three diffusion coefficients, but has no velocity or chemical potential gradient.

In FO, only concentration differences are considered as driving forces for mass transport. Chemical potential gradients of water and the draw solute are related to their concentration gradients as follows:

$$\nabla\mu = RT\frac{dln(a)}{dz} = \frac{RT\beta}{c}\frac{dc}{dz} \quad \text{with} \quad \beta = 1 + \frac{dln(\gamma)}{dln(c)} \tag{2}$$

The factor β accounts for solution non-ideality; for an ideal solute the chemical potential is directly proportional to a concentration gradient because both

the activity coefficient $\gamma = 1$ and $\beta = 1$. Integration of β yields the osmotic coefficient $\Phi(c)$ according to [23]:

$$\Phi(c) = \frac{1}{c}\int_0^c \beta dc = 1 + \frac{1}{c}\int_0^c c\, dln\gamma \tag{3}$$

The osmotic coefficient is conventionally indicated by the lowercase ϕ, but this is already in use to denote volume fractions. During integration, linear concentration gradients and linear volume fraction gradients are assumed. This is justified by the combination of relatively low fluxes encountered during FO and the small thickness of the active layer [24]. This assumption is explored in more detail in Supplementary Information.

The model derivation will be illustrated by means of the feed solute transport equation. In Eq. 2, the feed solute influence on the activity of water and draw solute will be ignored, as we assume a strongly diluted feed solution. For the feed solute itself, the chemical potential gradient is considered to be independent of feed solute concentration due to strong dilution ($\gamma_f(c_f) = 1$) but is influenced by the draw solute due to salting out. Salting out is the increase of a solute's activity due to the presence of inorganic ions in solution. The sensitivity of a feed solute towards salting out is captured by the Setschenow constant K^S for a given feed solute - inorganic salt pair, which is defined as [11]:

$$\frac{1}{c_d} log_{10}(\gamma_f) = K^S \tag{4}$$

with c_d and γ_f being the inorganic salt concentration and feed solute activity coefficient respectively. For NaCl, values of K^S of -0.068 to 0.354 L/mole have been found for a wide range of organic compounds [12]. Generally, K^S is higher for more apolar solutes and can be negative for highly polar solutes as well [11, 12]. Eq. 4 can be converted to:

$$\frac{dln\gamma_f}{dc_d} = K_e^S \tag{5}$$

in which the change of logarithm base is taken into account in the modified Setschenow constant K_e^S. In a multicomponent solution, the chemical potential gradient is differentiated to the local solution composition [20]:

$$\nabla\mu_f = RT\sum_{i=1}^{n-1}\frac{\partial lna_f}{\partial c_i}\frac{dc_i}{dz} \tag{6}$$

Due to the assumption of strong dilution, $\frac{dlna_f}{dc_w} = 0$, leaving:

$$\nabla\mu_f = RT\left(\frac{dln\, c_f}{dz} + \frac{dln\gamma_f}{dc_d}\frac{dc_d}{dz}\right) \tag{7}$$

Substitution of Eq. 5:

$$\nabla\mu_f = \frac{RT}{c_f}\frac{dc_f}{dz} + RTK_e^S\frac{dc_d}{dz} \tag{8}$$

Substitution of Eqs. 2 or 8 in Eq. 1 allows for integration between active layer interface concentrations of water, draw and feed solutes. Concentrations of all

species within the membrane are related to their concentrations at the interfaces by means of a partitioning coefficient K_i, in which continuity of the chemical potential is assumed [25]. For feed solutes, this yields:

$$K_f \Delta c_f + K_f \langle c_f \rangle K_e^S \Delta c_d = \sum_{i=1, i \neq f}^{n-1} \frac{\langle \phi_i \rangle \langle \phi_f \rangle (u_f - u_i) l}{\bar{v} Đ_{if}} \tag{9}$$

where $\langle \phi_i \rangle$ denotes the average volume fraction of component i in the membrane. Again, due to low fluxes, linear volume fraction gradients are assumed, and $\langle \phi_i \rangle$ is the arithmetic average of ϕ_i. Because $\langle \phi_f \rangle = \langle c_f \rangle \bar{v} K_f$, this equation can be further rearranged to:

$$\left(\sum_{i=1, i \neq f}^{n-1} \frac{\langle \phi_i \rangle}{Đ_{if}} \right)^{-1} \left(\frac{\Delta c_f}{l \langle c_f \rangle} + \frac{K_e^S}{l} \right) = u_f - \left(\sum_{i=1, i \neq f}^{n-1} \frac{\langle \phi_i \rangle}{Đ_{if}} \right)^{-1} \left(\sum_{i=1, i \neq f, m}^{n-2} \frac{\langle \phi_i \rangle u_i}{Đ_{if}} \right) \tag{10}$$

Filling in Eq. 10 for the three mobile components, we can define α_f as:

$$\alpha_f = \frac{Đ_{fm}}{\langle \phi_w \rangle Đ_{fd} Đ_{fm} + \langle \phi_d \rangle Đ_{wf} Đ_{fm} + \langle \phi_m \rangle Đ_{wf} Đ_{fd}} \tag{11}$$

such that Eq. 10 yields:

$$\frac{Đ_{wf} Đ_{fd} \alpha_f}{l} \left(\frac{\Delta c_f}{\langle c_f \rangle} + K_e^S \Delta c_d \right) = u_f - Đ_{fd} \alpha_f \langle \phi_w \rangle u_w - Đ_{wf} \alpha_f \langle \phi_d \rangle u_d \tag{12}$$

We can see that the driving force for velocity of the feed solute (concentration gradient over membrane thickness) is independent of feed solute partitioning into the membrane. The same is true for the other mobile species as well. This follows from the assumption of continuity of chemical potential across the membrane interfaces, which implies that the concentration gradients outside or inside the membrane interfaces are equivalent. Fluxes, however, are proportional to partitioning. Generally, solute or solvent velocities within the membrane are related to fluxes by:

$$J_i = c_i^M u_i = K_i c_i^F u_i \tag{13}$$

Superscripts M, F and P indicate membrane, feed and permeate compartments respectively, with the permeate and draw compartments being the same. The volumetric flux of water is given by:

$$J_v = u_w \langle \phi_w \rangle \approx u_w (1 - \langle \phi_m \rangle) \tag{14}$$

For feed solutes, rejection is calculated as follows: with $c_f^P = \frac{J_f}{J_v}$, substituting Eq. 13 in rejection yields:

$$R_f = 1 - \frac{K_f u_f}{J_v} \tag{15}$$

Integration of Eq. 1 for water and draw solutes is similar, using Eq. 2 instead of 8 for the chemical potential gradient. The resulting full system of equations for FO with water, feed solute and draw solute transport is given by:

$$\begin{bmatrix} \frac{Đ_{wf} Đ_{wd} \alpha_w}{\langle c_w \rangle l} \Delta (c_w \Phi(c_w)) \\ \frac{Đ_{wf} Đ_{fd} \alpha_f}{\langle c_f \rangle l} \left(\Delta c_f + \langle c_f \rangle K_e^S \Delta c_d \right) \\ \frac{Đ_{wd} Đ_{fd} \alpha_d}{\langle c_d \rangle l} \Delta (c_d \Phi(c_d)) \end{bmatrix} = \begin{bmatrix} 1 & -Đ_{wd} \alpha_w \langle \phi_f \rangle & -Đ_{wf} \alpha_w \langle \phi_d \rangle \\ -Đ_{fd} \alpha_f \langle \phi_w \rangle & 1 & -Đ_{wf} \alpha_f \langle \phi_d \rangle \\ -Đ_{fd} \alpha_d \langle \phi_w \rangle & -Đ_{wd} \alpha_d \langle \phi_f \rangle & 1 \end{bmatrix} \begin{bmatrix} u_w \\ u_f \\ u_d \end{bmatrix} \tag{16}$$

2.2. Support layer transport model

In the support layer, we assume sufficiently large pores so that multicomponent transport does not involve the membrane as a solution phase. Rather, the membrane is inert and merely defines the effective length over which transport phenomena take place, given by the structural parameter S (assumed $S = 400$ µm in the model). It follows that the solution is no longer highly dissimilar in terms of molar mass of its constituents, and a more conventional formulation of the Maxwell-Stefan model is used based on mole fractions (x_i) [18].

$$-\frac{x_i}{RT}\nabla\mu_i = \sum_{j=1,j\neq i}^{n-1} \frac{x_j J_i - x_i J_j}{c_t Đ_{ij}} \tag{17}$$

with c_t being the total molar concentration. Due to internal concentration polarization, the draw solute concentration decays exponentially towards the active layer. This implies that the composition of the draw solute, and thus all x_i, depends on the transmembrane coordinate z. Because x_f is very small, and $\sum x_i = 1$, it is assumed that $x_w = 1 - x_d$, and x_f is constant. For ideal solutions ($\beta = 1$), the analytical solution of the draw solute concentration as a function of transmembrane coordinate from $z = 0$ to $z = z$ is:

$$\begin{aligned} IF(z) &= exp\left(-\frac{z}{c_t}\left(\frac{J_w + J_d}{Đ_{wd}} + \frac{J_f}{Đ_{fd}}\right)\right) \\ x_d &= IF(z)^{-1}\left[\frac{J_d(Đ_{fd} + Đ_{wd}x_f)}{Đ_{fd}(J_w + J_d) + Đ_{wd}J_f}(IF(z) - 1) + x_{d1}\right] \end{aligned} \tag{18}$$

The derivation of Eq. 18 is given in Supplementary Information. When ignoring coupling with feed solutes ($Đ_{fd} = 1, J_f = x_f = 0$), Eq. 18 closely resembles common ICP equations such as those derived by Tiraferri et al. [26].
For feed solute transport in the support layer, Eq. 17 is rearranged so that J_f is a function of its different driving forces:

$$J_f = -\frac{c_f Đ_{fd} Đ_{wf}}{RT(x_w Đ_{fd} + x_d Đ_{wf})}\nabla\mu_f + \frac{x_f Đ_{fd}}{x_w Đ_{fd} + x_d Đ_{wf}} J_w + \frac{x_f Đ_{wf}}{x_w Đ_{fd} + x_d Đ_{wf}} J_d \tag{19}$$

This way, the contributions of the driving forces to J_f can be studied easily.

2.3. Relation between Fickian and Maxwell-Stefan diffusion coefficients

Membrane permeability and diffusion tests yield diffusivities according to Fick's law, as a proportionality coefficient between measured concentration differences and measured fluxes. To be able to use a M-S model, the Fickian diffusivities have to be converted, which is outlined in this section. From Eq. 2, it follows that Fickian and Maxwell-Stefan diffusivities can be transformed in one another by accounting for thermodynamic factors [18, 21]. In the case of solute diffusion tests, $Đ_{sm}$ can be calculated from measured Fickian diffusion coefficients (D_s, the solute diffusivity within the membrane). Generally, a steady-state solute flux through a membrane obeys [25]:

$$J_s = B\Delta c = \frac{D_s K_s}{l}\Delta c \tag{20}$$

with D_s and K_s being the hindered diffusion coefficient and solute partitioning coefficient. Starting from Eq. 1, developing an equation for solute diffusion yields:

$$-\frac{c_s}{RT}\nabla\mu_s = \left(\frac{\phi_s\phi_w}{\bar{v}Đ_{ws}} + \frac{\phi_s\phi_m}{\bar{v}Đ_{sm}}\right)u_s \tag{21}$$

In this equation, both water and membrane are considered stationary phases. For water, the absence of flux is justified by the relatively low solute concentration difference and film thickness typical for diffusion measurements. $\nabla\mu_s$ is transformed as shown by Eq. 2, and with $c_s\bar{v}/\phi_s = 1$ and $c_s u_s = J_s$, Eq. 21 is rearranged to:

$$-\beta\frac{dc}{dz} = \left(\frac{\phi_w}{Đ_{ws}} + \frac{\phi_m}{Đ_{sm}}\right)J_s \tag{22}$$

Integration yields:

$$J_s = \frac{Đ_{ws}Đ_{sm}K_s}{\langle\phi_w\rangle Đ_{sm} + \langle\phi_m\rangle Đ_{ws}} \cdot \frac{\Delta(c_s\Phi(c_s))}{l} \tag{23}$$

The osmotic coefficients in Eq. 23 can be substituted by a single factor defined as:

$$\Phi_s = \frac{c_s^F\Phi(c_s^F) - c_s^P\Phi(c_s^P)}{c_s^F - c_s^P} \tag{24}$$

so that substitution of J_s by Eq. 20 yields:

$$D_s = \frac{Đ_{ws}Đ_{sm}\Phi_s}{\langle\phi_w\rangle Đ_{sm} + \langle\phi_m\rangle Đ_{ws}} \tag{25}$$

Isolation of $Đ_{sm}$:

$$Đ_{sm} = \frac{\langle\phi_m\rangle Đ_{ws}}{Đ_{ws}\Phi_s - \langle\phi_w\rangle D_s}D_s \tag{26}$$

In the denominator of Eq. 26, the second term is usually very small compared to the first one, as $D_s << Đ_{ws}$ and $\langle\phi_w\rangle < 1$ while $\Phi_s \approx 1$ for dilute solutions. By omitting this second term, Eq. 26 simplifies to:

$$Đ_{sm} = \frac{\langle\phi_m\rangle}{\Phi_s}D_s \tag{27}$$

When diffusion tests are performed using very dilute solutions, the osmotic coefficients are approximately equal to 1, and $\langle\phi_m\rangle$ is also close to 1 for dense membranes, so $Đ_{sm}$ and D_s are approximately equal.
Similarly, the water diffusion coefficient within a membrane obtained from pressure-driven clean water flux tests can be related to $Đ_{wm}$. In the classical solution-diffusion model, the volumetric flux is related to membrane properties and the applied pressure difference as follows [25]:

$$J_v = \frac{K_w D_w \bar{v}}{lRT}\Delta P \tag{28}$$

In both the Maxwell-Stefan and classical solution-diffusion model, the chemical potential gradient is transformed into a water concentration gradient, with the concentration gradient caused by the pressure difference at both interfaces. This is because there is no pressure gradient within the active layer [25, 24]; the

pressure reduces discontinuously to the permeate pressure at the active layer - permeate interface. The resulting Maxwell-Stefan formulation is:

$$K_w c_w \left(1 - exp\left(-\frac{\bar{v}\Delta P}{RT}\right)\right) = \frac{\langle\phi_w\rangle\langle\phi_m\rangle u_w l}{\bar{v}Đ_{wm}} \tag{29}$$

which is simplified by Taylor expansion and with $K_w c_w \bar{v} = \langle\phi_w\rangle$ and Eq. 14 to:

$$J_w = \frac{\langle\phi_w\rangle Đ_{wm}\bar{v}}{\langle\phi_m\rangle lRT}\Delta P \tag{30}$$

Recognizing that for flux tests using pure water or dilute solutions $K_w = \phi_w$, we see that:

$$Đ_{wm} = \langle\phi_m\rangle D_w \tag{31}$$

2.4. Interactions between charged solutes

When using a mineral salt as a draw solute and with the feed solution containing charged solutes as well, there will be electrostatic interactions between ions on both sides of the membrane. The M-S diffusivity of the neutral species formed by an ionic feed solute and its draw solute counterion(s), does not depend on the ion-ion interaction, but is only determined by ion-water interactions of both cations and anions [18]. If one of the draw solute ions has a higher membrane permeability than its counterion, a transmembrane potential difference will develop according to the Nernst equation. The consequence of this potential is that charge neutrality is restored to the steady-state draw solute flux, due to acceleration and deceleration of the counter- and coions resp. The electrostatic potential gradient also influences the flux of charged feed solutes. It is assumed here that due to the much higher draw solute concentration compared to feed solutes that the draw solute flux determines the filtration potential. For charged solutes, the full transport equation then becomes [18, 19]:

$$-\frac{c_i}{RT}\left(\nabla\mu + z_i F\nabla\Psi\right) = \sum_{j=1, j\neq i}^{n-1} \frac{\phi_i\phi_j(u_i - u_j)}{\bar{v}Đ_{ij}} \tag{32}$$

The total transmembrane potential difference can be measured easily, but does not yield information on the local gradient. To the best of the author's knowledge, the electrostatic potential difference as a function of transmembrane coordinate has not yet been established for FO, and this is outside of the scope of this study. Generally, a filtration potential arises due to unequal ion permeability through the active layer and due to streaming current generated in the support layer [27]. Streaming current is the phenomenon where charged pore walls cause a charge separation of the ions in the pore liquid moving through the pores. This results in a deviation from net zero current of the fluxes of ionic species. However, due to the elevated salinity of FO draw solutions, electrical double layers are suppressed, and streaming current should be negligible [28]. For instance, for a 1-1 electrolyte such as NaCl, the Debye length at 0.1M concentration is less than 1 nm. Therefore, the filtration potential in FO will be due to unequal ion permeability of the active layer. Although the potential difference is caused by the active layer, the length over which the gradient is present is much larger, due to the influence of the resulting electromotive force

on draw solute ions in the vicinity of the active layer, thereby decreasing the gradient.

Measurements of the filtration potential during FO on CTA membranes by Bian et al. [29] using different draw solutes and membrane orientations, indicate that the filtration potential is limited to tens of mV, not exceeding 70 mV for multivalent draw solutes at high concentration differences. This fairly low filtration potential is likely the result of the low surface charge of CTA FO membranes, leading to similar permeance for cations and anions. TFC membranes hold more permanent surface charges, which should result in a higher filtration potential as well. Assuming that the potential difference is located across the active layer, the forces exerted by the concentration and potential gradients are in the same order of magnitude, showing the practical importance of electromigration in FO. This corresponds well with experimental reports of ion exchange in FO [2, 3, 4, 5, 6, 7].

Electromigration can be easily incorporated into the model detailed above by means of the additional driving force term of Eq. 32, but this requires that $\nabla\Psi$ is known. The frictional terms of Eqs. 1 and 32 are identical, only the driving force is increased or decreased (depending on valence). Electromigration was evaluated by varying $\nabla\Psi$ and calculating u_f for uncharged, cationic and anionic solutes. $\nabla\Psi$ was converted into non-dimensional form as $\nabla\psi_d = \nabla\Psi\frac{Fl}{RT}$, in order to allow for easy comparison with $\nabla\mu_f$.

3. Materials and methods

3.1. Active layer transport model

Initial values for ϕ_m, ϕ_w, Đ_{wm} and Đ_{dm} were based on studies by Freger [30], Geise et al. [31, 32] and Zhang et al. [33] and are listed in Table 1. The membrane characteristics are typical of somewhat looser desalination membranes: the modelled membrane had a polymer volume fraction of 0.9 and a thickness of 40 nm. The permselectivity of water over draw solute varied over a range of 100 - 10^5 due to varying K_d in the sensitivity analysis. The permselectivity of this membrane stems mostly from diffusional hindrance rather than low salt partitioning, as is the case for real membranes as well [31]. In all calculations, a membrane orientation of FO mode, active layer facing feed solution, was assumed. Eq. 16 is solved by guessing velocities, from which fluxes and interface concentrations are calculated. The interface concentrations are then used to recalculate velocities, and initial guesses are adjusted by a Nelder-Mead algorithm until convergence. A flow chart of the model solver is included in Supplementary Information. The draw solute was assumed to be NaCl. The binary water - NaCl M-S diffusion coefficient equals the Fickian NaCl diffusion coefficient at infinite dilution [18], being $1.55 \cdot 10^{-9}$ m^2/s. Draw solution non-ideality was not taken into account ($\Phi = 1$), as this is not the focus of this study and non-ideality is limited for NaCl in any case [34].

Volume fractions were calculated by assuming that each mobile species partitions into the membrane independently of other mobile species relative to their partitioning coefficient. The remaining volume is then assigned to the membrane phase. The thickness of the membrane is normalized afterwards, so that in all simulations the amount of polymer is the same, i.e. the product $l\langle\phi_m\rangle$ is a constant. Given that both feed and draw solutes are present only in relatively dilute solutions, the volume fractions are dominated by $\langle\phi_m\rangle$ and $\langle\phi_w\rangle$.

Table 1: Membrane and solution characteristics used in this study. The A and B coefficients are the water and NaCl permeability coefficients according to the classical solution-diffusion theory, calculated using Eqs. 20, 27, 28 and 31.

Parameter	Value	units
$Đ_{dm}$	$1{\cdot}10^{-13}$	m^2/s
$K_w\,(\approx \phi_w)$	0.1	-
$Đ_{wm}$	$1{\cdot}10^{-10}$	m^2/s
ϕ_m	0.9	-
l	40	nm
S	400	µm
c_d^P	1	mole/L
A	$2{\cdot}10^{-12}$	m/(Pa·s)
B	$4{\cdot}10^{-8}$	m/s

A water partitioning coefficient of 0.1 was used, which is a realistic value for both polyamide and cellulose ester-based membranes. The feed solution was assumed to be pure water containing an organic micropollutant at a concentration of 1 µM. Upon obtaining u_w, u_f and u_d, fluxes and feed solute rejection were calculated according to Eqs. 13 and 15.

3.2. Support layer transport model

Using Eq. 19, the different contributions to J_f are quantified. A feed solute concentration of 1 µM at the active layer - support layer interface is assumed (c_f^I), equal to the active layer model. A volume flux of about 20 LMH and RSF of $5.4{\cdot}10^{-5}$ mole/(m^2s) are used, as predicted by the active layer model for a 1M NaCl draw solution, with J_v converted to the molar water flux J_w. J_f is the sum of three components: two coupled contributions to water and the draw solute and one contribution of the feed solute's own chemical potential gradient. The contributions of J_w and J_d can be easily calculated, but the system is not determined: both J_f and $\nabla\mu_f$ are unknown and depend on each other. Interactions between the water, feed solute and draw solute fluxes in the support layer are then evaluated according to two scenarios: one in which the feed solute concentration gradient within the support layer is forced to zero, and one in which a fixed feed solute flux is enforced. The first scenario corresponds to the feed solute being transported through flux coupling only, while the second scenario corresponds to a fixed rate of feed solute permeating through the active layer. In both scenarios, $Đ_{fd}$ is varied from 10^{-15} to 10^{-9} m^2/s, $Đ_{wf} = 5{\cdot}10^{-10}$ m^2/s, and the response variables are the feed solute flux and feed solute concentration gradient within the support layer respectively. To formally link the feed solute flux through the active layer and support layer, an iterative process would be employed, where the feed solute interface concentration is estimated so that J_f through both layers is equal. This approach is however less informative than the scenarios outlined above, as the flux interactions within the support are partially obscured by the influence of transport through the active layer.

3.3. Sensitivity analysis

Sensitivity analysis was carried out using a full-factorial design followed by Sobol sensitivity index calculation. 6 factors were varied, being K_f, K_d, $Đ_{fm}$,

Table 2: Range of variation of variables used during full factorial sensitivity analysis.

Parameter	Range of variation	Fixed value in plots	units
K_d (NaCl)	0.001- 1	0.016	-
K_f	0.01 - 10	0.16	-
$Đ_{fm}$	$1 \cdot 10^{-14}$ - $1 \cdot 10^{-11}$	$6.3{\cdot}10^{-13}$	m^2/s
$Đ_{fd}$	$1 \cdot 10^{-13}$ - $1 \cdot 10^{-10}$	$2.5{\cdot}10^{-11}$	m^2/s
$Đ_{wf}$	$1 \cdot 10^{-11}$ - $1 \cdot 10^{-9}$	$4.0{\cdot}10^{-10}$	m^2/s
K^S	-0.075 - 0.3	0.075	-

$Đ_{wf}$, $Đ_{fd}$ and K^S. The response variable was feed solute rejection in all cases. In order to carefully study feed solute - draw solute interactions, the range of variation for the draw solute-related factors was especially broad. K_d for instance is varied from 0.001 to 1, with the values on the upper end of the interval being unrealistically high: K_w was fixed at 0.1, so at the upper end of the K_d interval, the membrane would preferentially take up draw solute rather than water. Clearly, such a membrane would make for a poor FO membrane. Each factor was varied over six levels, yielding a 6-dimensional solution space. Only six levels were examined due to the high computational cost of the full-factorial design. A full factorial design was implemented rather than Monte Carlo sampling, because the full factorial design allows for easier interpretation of the obtained feed solute rejection.

Because all factors except K^S were varied over multiple orders of magnitude, factors were varied according to a geometric series, so that:

$$\frac{f_{n+1}}{f_n} = c \Leftrightarrow f_n = f_1 \cdot r^{\left(\frac{n-1}{e-1}\right)} = f_1 \cdot c^{(n-1)} \tag{33}$$

With f_1, r, e and c being the lowest value of factor f, the range of variation, the number of elements of factor f and the constant ratio of two subsequent elements of f respectively. K^S was varied from -0.075 to 0.3, which roughly corresponds to the range of variation found by Ni et al. [12] for many organic compounds in the presence of NaCl.

Sobol sensitivity indices were calculated for single variables and interaction between two variables. The Sobol method relies on quantifying the contribution of variables or interaction between variables to the variance of the response variable [35, 36, 37]. A function $f(x)$ with n independent variables defined in I^n is assumed to be composed of summands of increasing dimensionality:

$$f(x) = f_0 + \sum_{i=1}^{n} f_i(x_i) + \sum_{i=1, i<j}^{n} f_{ij}(x_i, xj) + ... + f_{12...n}(x_1, x_2, ..., x_n) \tag{34}$$

With the condition of every integral of a summand over any of its independent variables equalling zero, Eq. 34 can be written for interactions of two variables as:

$$\int f(x) \prod_{k \neq i,j} dx_k = f_0 + f_i(x_i) + f_j(x_j) + f_{ij}(x_i, x_j) \tag{35}$$

Squaring and integrating leads to the following definitions of variances:

$$D = \int f^2 dx - f_0^2 = Var(f(x))$$
$$D_{i_1 \dots i_s} = \int f_{i_1 \dots i_s}^2 dx_{i_1} \dots dx_{i_s} = Var(E(f(x)|x_{i_1 \dots i_s})) - \sum^{s-1} D_{i_1 \dots i_{s-1}} \tag{36}$$

Finally Sobol sensitivity indices were calculated as:

$$S_i = \frac{D_i}{D} \tag{37}$$

4. Results and Discussion

4.1. Obtained fluxes and sensitivity

Water and draw solute fluxes as a function of draw solute concentration are shown in Figure 1. Note that the draw solute concentration difference here is across the active layer only, so there is no ICP, which is why the fluxes are approximately linearly proportional to draw solute concentration. Also shown is feed solute rejection calculated using the fixed values for the different feed solute M-S diffusion coefficients and partitioning given in Table 2.

During active layer transport, the dominant influence on feed solute rejection was found for $Đ_{fm}$ and K_f, being the inverse feed solute - membrane friction coefficient and feed solute partitioning respectively, which predicted rejection to vary from slightly negative values to unity for the range of variation of these factors. A 3D slice of the solution is shown in Figure 2; see Table 2 for the fixed values of the other factors. In dense membranes, $\langle \phi_m \rangle$ is the dominant volume fraction and can be in excess of 95% [30]. It follows that frictional hindrance between the feed solutes and other components will be dominated by $Đ_{fm}$. It was also found that the influence of $Đ_{fm}$ and K_f takes precedence over other variables influencing rejection. This implies that if $Đ_{fm}$ and/or K_f would cause rejection to be high, rejection would indeed be high regardless of other factors. Only when $Đ_{fm}$ and K_f allow for low rejection, can the other factors affect rejection. This can be explained as follows. With $J_f = c_f K_f u_f$, and u_f mainly determined by $Đ_{fm}$, J_f can be constrained by both partitioning and feed solute velocity. Either one of these two variables can be very small, resulting in negligible J_f, regardless of influences on the other variable.

Aside from feed solute partitioning and feed solute - membrane friction, salting out also had a significant influence on rejection, albeit smaller than the former factors. Salting out of feed solutes causes the driving force for transport to decrease by increasing the activity coefficient of feed solute molecules which have passed into the draw solution, thereby increasing feed solute rejection. Conversely, salting in could lower rejection, but salting in is much less common than salting out. This is shown in Figure 3, where in the case of low solute-membrane friction on the lower left side of the graph negative rejection was obtained (-6%) with salting in, while in the case of strong salting out, rejection was still significant at 53%. On the other hand, if solute-membrane friction is high (upper right side), rejection only varied between 98 and 99%, showing again the dominance of $Đ_{fm}$ over other factors.

The remaining factors, $Đ_{fd}$, $Đ_{wf}$ and K_d, turned out to be insignificant over their range of variation. This means that frictional coupling between feed

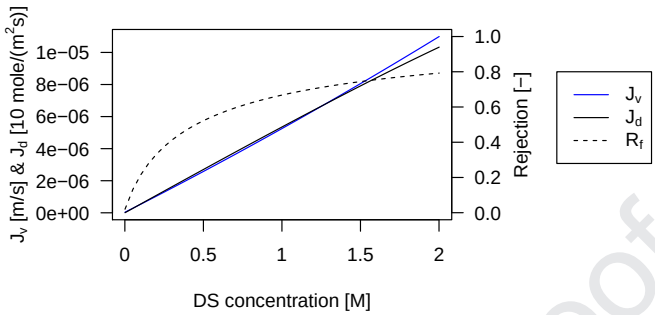

Figure 1: Volume and draw solute fluxes (J_v and J_d) and feed solute rejection (R_f) as a function of draw solute concentration. Note that only active layer transport is included so that there is no ICP, which is why the fluxes are linearly proportional to draw solute concentration.

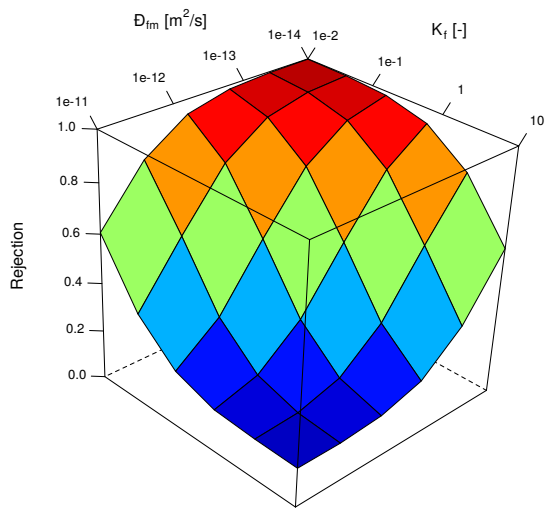

Figure 2: Rejection as a function of $Đ_{fm}$ and K_f, the variables determining feed solute rejection. Rejection varies from 16% to 100% in this graph.

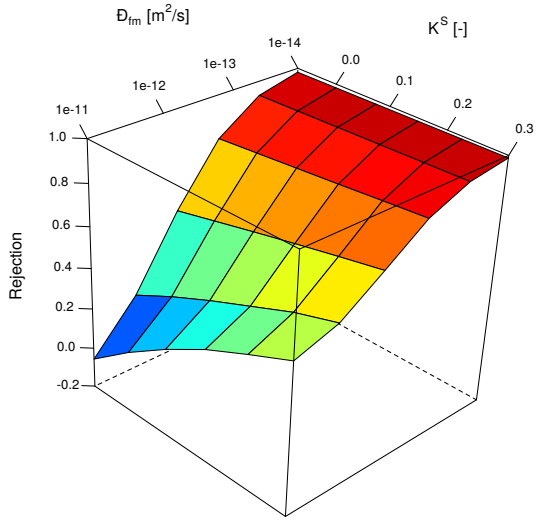

Figure 3: Rejection as a function of $Ð_{fm}$ and K^S. Slight negative rejection (-6%) was obtained when feed solutes were subject to salting in and when solute-membrane friction was low.

solutes, water and draw solute does not significantly influence feed solute transport across the active layer. Rejection as a function of $Ð_{fd}$ and K_d is shown in Figure 4, where rejection only varied from 34.5 to 38.0%. It should be stressed that in Figure 4, rejection showed the highest sensitivity towards K_d when K_d was unrealistically high. At $K_d = 0.1$ to 1, the membrane would take up draw solute in favour of water (with $K_w = 0.1$), resulting in a low permselectivity of 1000 to 100.

The figures presented above are slices from the 6-dimensional solution space, so they cannot convey the total impact of a factor on rejection. To overcome this limitation, variance analysis using the Sobol method was used. A first indication of significance of a factor is gained by reducing the dimensionality by fixing one factor and calculating the variance of the remaining solution space. The result of this is shown in Figure 5, with the blue dashed line being the variance of the entire solution space. It is immediately apparent that any change in variance is due to three factors, $Ð_{fm}$, K_f and K^S, while the remaining three factors, $Ð_{wf}$, $Ð_{fd}$ and K_d do not alter the variance of their solution subspaces. The Sobol sensitivity indices confirm the above analysis: S_i were 0.46 and 0.48 for $Ð_{fm}$ and K_f respectively, 0.09 for K^S and <0.001 for the other factors, shown in Figure 6. Sobol sensitivity indices for interaction between two variables showed that $Ð_{fm}$ and K_f do not interact. All S_{ij} containing either $Ð_{fm}$, K_f or both were almost equal. The lack of interaction can be explained by $Ð_{fm}$ and K_f being coefficients of distinctly different physical processes.

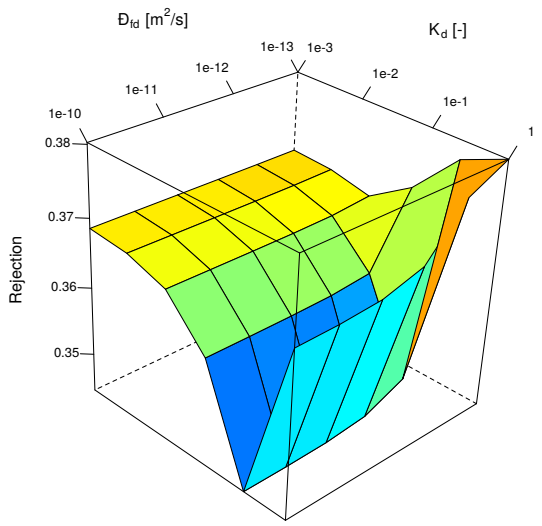

Figure 4: Rejection as a function of D_{fd} and K_d. Note that the overall influence of draw solute properties on feed solute rejection is low, and for realistic values of K_d (<0.1), the influence is much lower still.

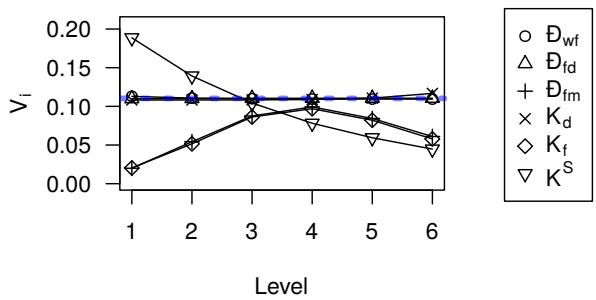

Figure 5: Variance of feed solute rejection in solution subspaces when one factor was fixed. Variance of the entire solution space is given as the dashed blue line.

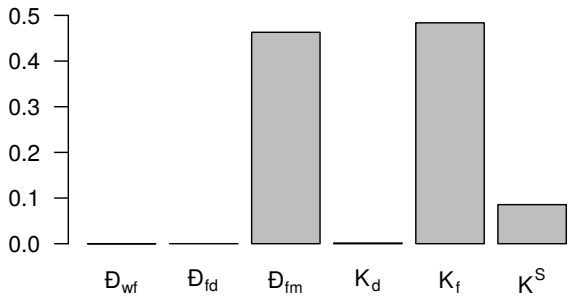

Figure 6: Sobol sensitivity indices for the six factors, clearly showing that rejection is determined mainly by $Đ_{fm}$ and K_f, in about equal measure. K^S is of secondary importance, while the other factors, $Đ_{fd}$, $Đ_{wf}$ and K_d, have no significant influence on rejection.

4.2. Flux coupling during active layer transport

The Sobol sensitivity analysis showed quantitatively that frictional coupling between different mobile species is insignificant, and accounted for only about 0.1% of the variance in rejection. For dense membranes, the insignificance of flux coupling is not surprising. It is in fact one of the assumptions made in the classical solution-diffusion model [25]. The low sensitivity of feed solute rejection towards coupling was also shown for salt rejection by seawater RO [24]: even in the case of strong frictional coupling versus no coupling, the difference in salt rejection is limited to less than 1%. This lack of flux coupling due to solute - membrane friction can be shown in this model too. If we assume for all mobile species that frictional drag predominantly comes from solute - membrane drag, it follows that $Đ_{im} < Đ_{ij}$ and $\langle\phi_m\rangle > \langle\phi_i\rangle$. Then, returning to Eq. 11, we can simplify the denominator accordingly to:

$$\alpha_f \approx \frac{Đ_{fm}}{\langle\phi_m\rangle Đ_{wf} Đ_{fd}} \tag{38}$$

Disregarding salting out for clarity, the feed solute transport equation of Eq. 16 then simplifies to:

$$\frac{Đ_{fm}}{l\langle\phi_m\rangle}\frac{\Delta c_f}{\langle c_f\rangle} = u_f - \frac{Đ_{fm}\langle\phi_w\rangle}{Đ_{wf}\langle\phi_m\rangle}u_w - \frac{Đ_{fm}\langle\phi_d\rangle}{Đ_{fd}\langle\phi_m\rangle}u_d \tag{39}$$

Eq. 39 still contains flux coupling terms, but again for $Đ_{im} < Đ_{ij}$ and $\langle\phi_m\rangle > \langle\phi_i\rangle$, the coefficients of u_w and u_d vanish, leaving only a diffusive contribution to u_f, in agreement with the classical solution-diffusion model. Subsequently, c_f^P can be eliminated using Eq. 13 and with Eq. 15, rejection can expressed as a function of water flux and the feed solute permeability coefficient ($= B = \frac{Đ_{fm}K_f}{\langle\phi_m\rangle l}$):

$$R_f = 1.5 + \frac{B}{J_v} - \frac{\sqrt{J_v^2 + 12BJ_v + 4B^2}}{2J_v} \tag{40}$$

Eq. 40 tends to 0 and 1 for J_v tending to 0 and $+\infty$, as expected. If salting out is included, the derivation remains unchanged, apart from adding a salting out term to the solute transport driving force ($K_e^S \Delta c_d$). For ease of notation, setting $K_e^S \Delta c_d = \sigma$, the following equation of solute rejection as a function of volume flux was obtained:

$$R_f = 1.5 + \frac{B}{J_v} - \frac{\sigma B}{2J_v} - \frac{\sqrt{J_v^2 + (12 + 2\sigma)BJ_v + B^2(4 - \sigma^2 - 4\sigma)}}{2J_v} \tag{41}$$

This equation describes feed solute rejection as a function of volume flux and salting out, with the feed solute flux uncoupled from all other fluxes. An example of the effect of salting out on feed solute rejection is shown in Supplementary Information, in which the rejection of a fairly high permeance solute varies by about 10% depending when K^S is varied between 0 and 0.3. In Figure 7, rejection is shown for both feed solute-membrane friction being dominant and for the simplification of uncoupled fluxes (Eq. 40), being the blue and dotted lines respectively. Both graphs completely overlap, showing that in this case the feed solute flux is de facto uncoupled from other fluxes.

The assumptions leading to the above simplification are of course only valid if feed solute - membrane friction dominate over other frictional drag sources. For small organic compounds, not much larger than a water molecule, this assumption can be invalid. In that case, $Đ_{wm} \approx Đ_{fm}$ and $Đ_{fm}$ would be not much smaller than $Đ_{wf}$. This case is illustrated as the dot-dashed line in Figure 7, showing rejection as a function of J_v for all $Đ_{ij} = 1{\cdot}10^{-10}$ m^2/s. Rejection in this case is very low, and hardly increases with increasing water flux. In a previous study, [8], we have shown evidence for significant frictional coupling between water and small mono-alcohols in FO membranes. The extent of flux coupling with water was high for primary alcohols, but quickly diminished as the steric hindrance of the alkyl chain increased due to branching, with flux coupling being almost absent for tertiary alcohols such as tert.butanol. Applying these findings to typical OMPs, such as pharmaceuticals or pesticides, it is unlikely that flux coupling between water and OMPs has a measurable impact on rejection. Many OMPs are significantly larger than the alcohols mentioned above, and thus feed solute-membrane friction will dominate over flux coupling. However, should a more permeable membrane be used in combination with a large MW draw solute, coupling with water flow will occur with larger feed solutes too.

Should there be flux coupling, then due to the molar flux of water being many orders of magnitude larger than the draw solute flux, any significant frictional flux coupling will involve the water flux, ruling out significant frictional feed solute - draw solute interactions. This is illustrated by the solid black line, where all M-S diffusivities were considered small (high friction) and equal, resulting in about 6% lowered rejection. This is in line with the conclusions of the Sobol analysis of the previous section as well. Even when $Đ_{fd}$ would be the dominant friction factor, the effect on rejection is here predicted to be minimal. Maintaining high feed solute-membrane friction but applying a feed solute-draw solute friction which is two orders of magnitude stronger (i.e. , $Đ_{fm} = 1{\cdot}10^{-13}$, $Đ_{fd} = 1{\cdot}10^{-15}$ m^2/s), the dashed curve is obtained, which results in at most 2% increased rejection. Note that this case assumes unrealistically high feed solute-draw solute friction, as will be shown in Section 4.4. It should also be mentioned that different friction factors can correlate. For instance, by lowering

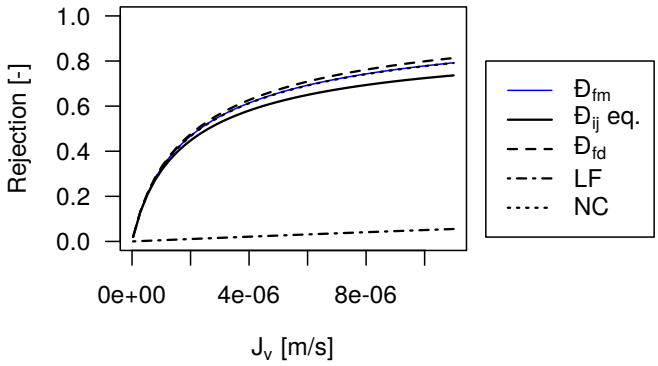

Figure 7: Rejection calculated for different cases of $Đ_{ij}$. From top to bottom: $Đ_{fm}$ = main hindrance from feed solute - membrane friction, $Đ_{ij}$ eq. = all friction coefficients high and equal, $Đ_{fd}$ = main hindrance from feed solute - draw solute friction, LF = low friction; all friction coefficients low and equal, NC = no coupling, rejection calculated according to Eq. 40. Note, $Đ_{fm}$ and NC overlap.

$Đ_{wf}$ in our model, flux coupling with water can become significant, however, in reality, compounds exhibiting low diffusivity tend to be large compounds and would thus exhibit a very low $Đ_{fm}$ as well.

4.3. Transport in the support layer

Flux coupling is pronounced during transport in the support layer, in contrast to transport through the active layer. Feed solute flux hindrance within the support layer can contribute to feed solute rejection: should strong hindrance take place between the draw solute and feed solutes, then the feed solute concentration would remain relatively high at the active layer - support layer interface, which in turn diminishes the feed solute concentration difference across the active layer, causing an overall decrease of J_f and increased rejection. In contrast to active layer transport, there is no $Đ_{im}$ dwarfing all other frictional interactions, because the support layer is porous. In the absence of $Đ_{im}$, it is quite likely that feed solute - draw solute friction is in fact the largest friction factor, given that both solutes are larger than water. Additionally, the support layer is about three orders of magnitude thicker than the active layer and contains a higher draw solute concentration, allowing for more frictional feed solute - draw solute interaction.

As mentioned in Section 3.2, frictional interactions between water, draw solute and feed solute fluxes are studied by either fixing the feed solute concentration gradient to zero (scenario 1) or flux within the support layer (scenario 2) and by varying $Đ_{fd}$ from 10^{-15} to 10^{-9} m^2/s. The response variables are the feed solute flux and concentration gradient respectively. The results of the first scenario are shown in Figure 8, where $\nabla\mu_f = 0$ and the normalized contributions of J_w and J_d to J_f are shown as a function of $Đ_{fd}$, as well as the resulting normalized J_f. Note that the contribution of J_d is negative; it is shown as absolute

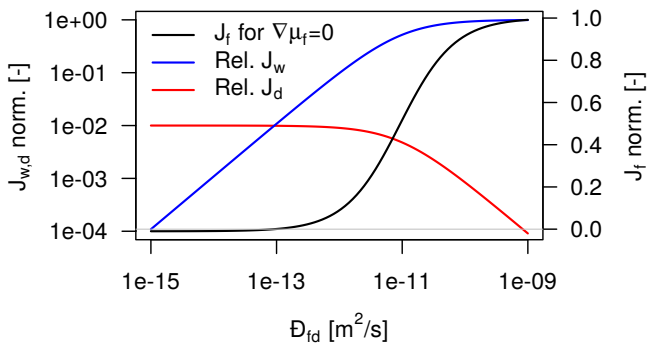

Figure 8: Normalized contributions of J_v and J_d to J_f as a function of $Đ_{fd}$ and the normalized J_f needed to maintain equal feed solute concentration throughout the support layer after permeating through the active layer. All fluxes are normalized to J_f when fully coupled with water only, i.e. $J_f = J_v c_f^P$.

value in Figure 8. It can be seen that for $Đ_{fd} < 10^{-13}$ m^2/s, J_f is in fact slightly negative, meaning that the draw solute flux would entrain permeated feed solute towards the active layer. In this case, the draw solute in the support layer would strongly hinder feed solute permeation. For $Đ_{fd} > 10^{-10}$ m^2/s, the influence of feed solute - draw solute friction on J_f becomes negligible, which also implies that feed solute rejection is then only determined by resistance in the active layer. The calculations of the second scenario are shown in Figure 9, where a fixed J_f was enforced and the resulting ∇c was calculated. Similar to the first scenario, hindrance due to the draw solute flux is significant for low $Đ_{fd}$ values, but becomes negligible when $Đ_{fd}$ approaches $Đ_{wf}$. As a reference: the concentration gradient of a fully rejected feed solute across the active layer, present at a concentration of 1 µM, is in the order of 10^4 moles/m^4, so only at very small $Đ_{fd}$ values can hindrance induced by the draw solute match the hindrance imposed by the active layer.

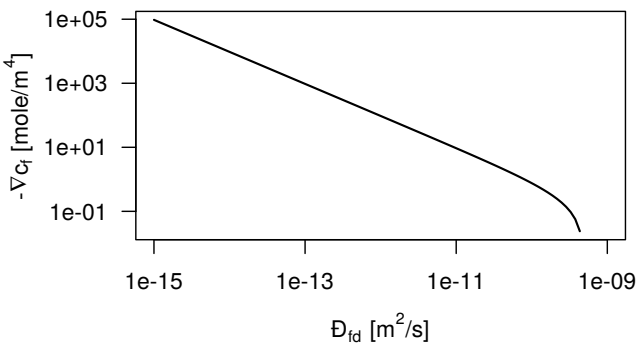

Figure 9: Concentration gradient of permeated feed solute within the support as a function of $Đ_{fd}$ when a feed solute flux is enforced. Here, the presence of a concentration gradient implies that draw solute friction contributes to overall resistance against feed solute transport, and vanishes for high $Đ_{fd}$.

4.4. Feed solute - draw solute interactions

In the previous sections, the importance of coupling between feed solutes and the draw solute sometimes hinged on the value of $Đ_{fd}$. Unfortunately, there is very little data available on the friction between salts and organic compounds, but there are indications that this friction factor not significantly greater than other solution friction factors. Using simultaneous Taylor dispersion of two compounds, Leaist [38] studied the Fickian diffusion of sucrose and KCl, finding that KCl enhanced the diffusion of sucrose. Of course, the increased diffusivity of sucrose can also be due to salting out, as Fickian diffusion coefficients account for both frictional interactions and solution non-ideality. It does show however, that if there is increased frictional hindrance, it must be smaller than the effect of salting out. Given that sucrose is a strongly hydrophilic solute, salting out is expected to be minimal [12], indicating that KCl-sucrose friction will be small as well. Another indication, albeit indirect, is by diffusion tests carried out by Sauchelli et al. [10], using two TFC FO membranes and organic micropollutants. The diffusion tests were carried out both in deionized water and salt solutions. Some electrostatic interactions between charged OMPs and salts were seen, but the permeance of the uncharged OMPs through the FO membranes was unaltered. These results again indicate that frictional interactions between feed and draw solutes are not important.

We have measured the self-diffusion of atenolol (MW 266.33 g/mole) as a tracer in NaCl-D_2O (deuterium oxide) solutions between 0 and 4M NaCl using pulsed field gradient NMR according to the method described by Ma et al. [39]. It was found that the self-diffusion decreased slightly from 0.46 to $0.36 \cdot 10^{-9}$ m^2/s as a function of salinity, shown as the black data series in Figure 10. Self-diffusion is proportional to the inverse of solution viscosity according to the Stokes-Einstein relation, and is not influenced by solution non-ideality, because of the absence of a salinity gradient within the homogeneous solution. After accounting for the increased viscosity of concentrated NaCl solutions [40], the self-diffusion is

converted into the blue data series in Figure 10, now in units of N. It can be seen that this viscosity-corrected self-diffusion coefficient is nearly independent of the NaCl concentration; it varies only by 3% and increases slightly with increasing NaCl concentration rather than decreasing. The increased diffusivity could stem from the viscosity of NaCl - D_2O solutions deviating from NaCl - H_2O solutions, or from reduced hydration of the organic solute [11]. The measured Fickian diffusion coefficient can be related to M-S diffusivities as follows. By considering that the system is at equilibrium, it follows that all forces exerted on water, NaCl and atenolol must cancel out: $\sum F_i = 0$ [17, 22]. A small perturbation to atenolol will cause a small velocity difference relative to the surrounding water and NaCl. The latter two components are present at much higher concentrations, and thus they can be considered stationary due to no net force being exerted. This yields:

$$-\nabla\mu_f = \frac{RTx_w u_f}{Đ_{wf}} + \frac{RTx_d u_f}{Đ_{fd}} = RTu_f\left(\frac{x_w}{Đ_{wf}} + \frac{x_d}{Đ_{fd}}\right) \tag{42}$$

Multiplying both sides by $c_t x_f$ and expressing the driving force as a concentration gradient according to Eq. 2 yields:

$$J_f = -\left(\frac{x_w}{Đ_{wf}} + \frac{x_d}{Đ_{fd}}\right)^{-1}\nabla c_f \tag{43}$$

Note that feed solute non-ideality does not appear in Eq. 43 due to the absence of an activity coefficient gradient. Equating the self-diffusion to the M-S diffusivities, one arrives at [41, 42]:

$$D = \frac{Đ_{fd}Đ_{wf}}{x_w Đ_{fd} + x_d Đ_{wf}} \tag{44}$$

This yields $Đ_{fd} = 8.8\pm0.9\cdot10^{-11}$ m^2/s. Returning now to Figures 8 and 9, it can be seen that frictional hindrance at this value for $Đ_{fd}$ is quite low. From these calculations and the literature mentioned earlier, it can be concluded that frictional hindrance within the support is minimal for OMPs and small draw solutes. The data set presented here is very limited in size, a more systematic study is warranted. It is conceivable that feed solute - draw solute combinations are possible where frictional hindrance is significant.

The importance of electromigration for charged feed solutes was assessed by means of Eq. 32, in which the driving force for feed solute transport is the electrochemical potential gradient, rather than only the chemical potential gradient. Given that the electrostatic potential as a function of transmembrane coordinate is unknown, an estimate for the upper limit of the potential difference across the active layer was made. For a membrane showing perfect permselectivity between anions and cations for a 1-1 salt, and at a concentration ratio of 100 between feed and draw, the total potential difference would be equal to the Donnan potential of 118 mV. This concentration ratio is attainable in FO, but FO membranes are not close to being perfectly permselective, decreasing the effective potential difference. Therefore, the upper limit was set to 40 mV, in range with the values reported by Bian et al. [29]. Feed solute velocity for neutral, anionic and cationic solutes is reported in Figure 11 as a function of the non-dimensional electrostatic potential gradient ($\nabla\psi_d = \nabla\Psi\frac{Fl}{RT}$). The concentration gradient in non-dimensional form is $\frac{\Delta c_f}{\langle c_f\rangle}$, which can be at most two for

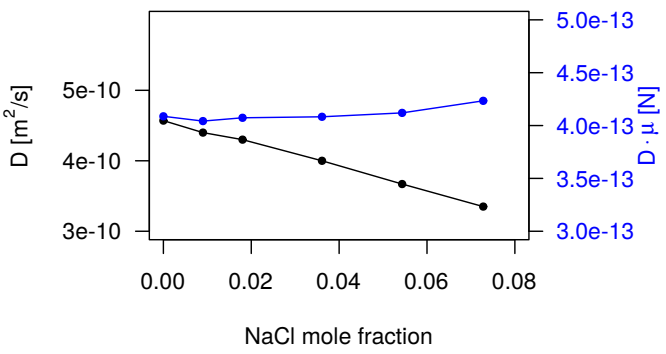

Figure 10: Self diffusivity of atenolol as a function of NaCl concentration in D_2O (black) and after correction for solution viscosity (blue).

complete rejection. At $\psi_d = 1$, the electrostatic potential across the active layer is 26 mV. At this potential, velocity of co-ions and counterions is 46% and 164% of the velocity of neutral solutes respectively, showing that electromigration is a significant driving force in FO.

In the current model, certain feed solute - draw solute interactions are not yet included. Draw solutes can alter feed solute - membrane affinity, thereby altering feed solute partitioning into the membrane (K_f). In a previous publication, we reported on a dramatic change in feed solute rejection when comparing FO and RO operation of the same membrane and same feed solutes [8]. This resulted in negative rejection of the feed solutes during FO, despite salting out of the feed solutes. Such interactions are unfortunately hard to predict and are specific to certain feed solute, draw solute and polymer combinations. K_f was shown to be of primary importance for feed solute rejection in this study, but it was considered independently of draw solute type and concentration. Another interaction which is not included is the effect of the draw solute on feed solute - membrane friction ($Đ_{fm}$). These interactions include active layer swelling or shrinking, dehydration of organic solutes and modification of the de facto pore size distribution due to ions blocking smaller pores. The influence of salinity on organic feed solute rejection has been studied in detail in nanofiltration, where it was found that saline feeds cause decreased organic solute rejection [13, 14, 15, 16]. Although active layer swelling is often proposed to explain reduced organic solute rejection, it has been contradicted by direct measurement of active layer swelling and the decreased rejection has been shown to occur also in ceramic membranes [14], which can be reasonably assumed to be rigid. Freger [30] showed that polyamide layers swell considerably less in brines compared to DI water, and that permeability of a membrane correlates strongly with the degree of swelling. In a previous study, we also reported that the water permeability of CTA FO membranes declines with increasing draw solute osmotic pressure, although this was not seen in TFC FO membranes [40]. It is also well-known that the diffusivity of solutes strongly depends on their size relative

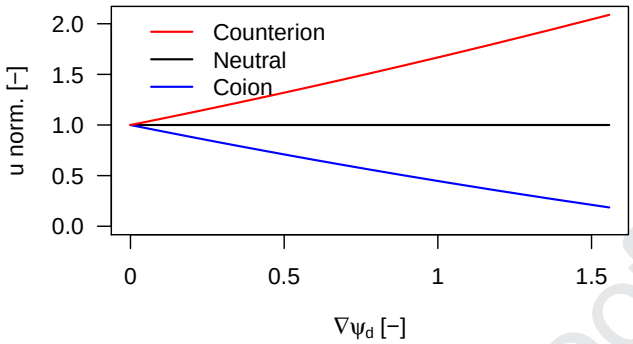

Figure 11: Normalized feed solute velocity as a function of non-dimensional electrostatic potential gradient for counterions, coions and neutral solutes.

to membrane pore sizes. For instance, Dražević et al. [43] directly measured hindered diffusivity of several organic solutes in the active layer of a SWC4+ RO membrane, finding that solute diffusivity decreased by almost two orders of magnitude when the Stokes radius increased from 0.20 to 0.27 nm. With respect to dehydration, it should be mentioned that FO operates based on lowering water activity to a level below that of the feed solution, which may already be at reduced activity. RO and NF on the other hand, operate based on increasing the water activity beyond that of the permeate, being (relatively) pure water. Active layer dehydration could then be expected to be of greater importance in FO than in pressure-driven systems. However, there is some proof that membrane compaction due to hydrostatic pressure also leads to decreased membrane permeability and increased feed solute rejection. Kong et al. [9] studied the permeance of 24 pharmaceutical compounds in CTA FO membranes, operated as FO, RO and diffusion only, and modelled the results according to the solution-diffusion model. They found that generally permeances obtained using RO were lower (i.e. higher OMP rejection) compared to FO and diffusion, which they attributed to active layer compression due to hydrostatic pressure in RO. Similarly, Tiraferri et al. [26] found that NaCl permeance by FO membranes decreased significantly when operated as RO, and was tentatively attributed to compaction as well. Using cross-sectional SEM micrographs of different nanocomposite membranes, Pendergast et al. [44] were able to confirm compaction of the support layer, which they relate to increased rejection by means of an increased path length through the active layer from the feed side to shrunken support-free zones on the permeate side. Given that there is no hydrostatic pressure applied in FO, support compaction would be absent. Apparently, both pressure- and osmotically-driven operation have specific mechanisms by which membrane permeability declines.

The lowered organic solute rejection in saline NF feeds can be satisfactory explained by salting out. Dehydration of the organic solutes decreases their effective size, which is one of the mechanisms of salting out and also reduces their

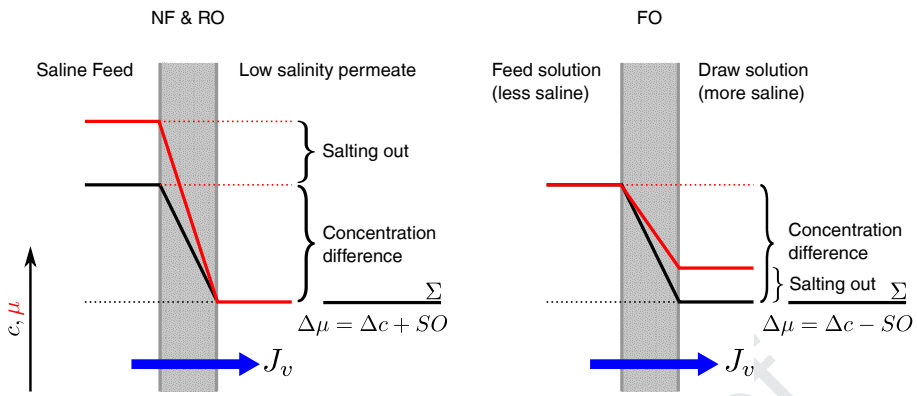

Figure 12: Schematic illustration of the influence of salting out on the driving force for feed solute rejection in pressure-driven systems (left side) and FO. In the pressure-driven case, the feed solute concentration and salinity gradients share the same direction and are thus additive, while in the case of FO, they are oppositely directed and thus counteract each other.

effective size. Alternatively, if the solute needs to shed its hydration shell in order to be able to pass through the active layer, the activation energy for partitioning into the membrane is lowered if the hydration shell is already weakened by salting out [45]. The NF tests on saline feeds containing organics are different from the FO case at hand: the direction of the salinity gradient is switched relative to the direction of feed solute flux through the membrane. In the NF case, salting out then decreases feed solute rejection but in the FO case, rejection is increased by salting out. This is illustrated schematically in Figure 12. Xie et al. [1] systematically studied FO and RO operation of the same membrane with a feed solution containing hydrophobic OMPs. They found a correlation between reverse draw solute flux and OMP rejection, and interestingly, also found that during FO, adsorption of OMPs onto the membrane was decreased. The increased rejection during FO operation was then ascribed to frictional hindrance between OMPs and the draw solute. Given the results of the sensitivity analysis presented here, a more likely explanation of these findings would be a change in feed solute partitioning and salting out.

5. Conclusions

This study presents a comprehensive FO transport model based on Maxwell-Stefan theory for feed solute transport. It includes frictional interactions with all components of the system, feed solute non-ideality due to salting out and electromigration. Feed solute transport through the active layer was found to be de facto uncoupled from other fluxes, and was determined by friction with the membrane polymer and partitioning into the membrane. Of significant but secondary importance was salting out, as this decreases the effective driving force for feed solute transport. The draw solute was found to not have noticeable frictional interactions with feed solute transport, even at unrealistically high feed solute - draw solute friction or excessively high draw solute partitioning. Should the solute - membrane friction be less (more permeable membrane), flux coupling with water is more likely to occur, as the water flux is orders of magnitude larger than the draw solute flux, and draw solute partitioning into the

active layer is generally low. Feed solute partitioning can also be influenced by draw solute and draw solution concentration, but was considered independently in this model. When comparing FO, RO and diffusive operation of the same membrane, differences in feed solute partitioning should be taken into account in order to provide a fair comparison of feed solute permeance in the different processes.

Electromigration is shown to be an important driving force for transport of charged solutes, with the necessary electrostatic potential difference being generated by draw solute diffusion itself. This is true under the condition that most of the electrostatic potential gradient is located across the active layer only. In that case, the resulting driving force can match the driving force generated by the solute's concentration gradient. This is likely the case, given that ion exchange has been observed experimentally.

During transport through the support layer, there is significant flux coupling, as solute - membrane friction is no longer dominant and path length has increased by about three orders of magnitude compared to the active layer. It is shown that frictional coupling between OMP feed solutes and NaCl has a small effect on OMP transport. Theoretically, significant feed solute - draw solute coupling is possible in the support layer, although this likely requires larger draw solutes resulting in higher friction factors.

6. Acknowledgements

Dr. Paolo Sabatino is kindly acknowledged for performing the pulsed-field NMR self-diffusion measurements of atenolol.

7. List of symbols

A - Membrane water permeability according to the classical solution-diffusion model

B - Membrane solute permeability according to the classical solution-diffusion model

$c_{f,d,w}$ - Molar concentration of feed solute, draw solute or water resp.

$c_i^{F,M,I,P}$ - Molar concentration of component i in the feed, active layer, interface between active layer and support layer and permeate/draw solution resp.

c_t - Total molar concentration of solution

$Đ_{ij}$ - Maxwell-Stefan binary diffusivity of components i and j

D_i - Sobol variances of factor i

D_s, D_w - Diffusivity of solute and water resp. according to Fick

J_i - Molar flux of component i

J_v - Volume flux

K_i - Distribution coefficient of component i

K^S - Setschenow constant

l - Thickness of the active layer

P - Pressure

R_f - Rejection of feed solute

R - Gas constant

S_i, S_{ij} - Sobol sensitivity indices of component i and i, j interacting resp.

S - Membrane structural parameter

T - Absolute temperature
u_i - Velocity of component i
$\bar{v}$ - Molar volume
x_i - Molar fraction of component i
z_i - Charge of solute i
z - Transmembrane coordinate

Greek letters
α_i - Coupling coefficient of component i
β - Differential osmotic coefficient
μ - Chemical potential
ϕ - Volume fraction
Φ - Osmotic coefficient
Ψ - Electrostatic potential
ψ_d - Dimensionless electrostatic potential

8. References

[1] M. Xie, L. D. Nghiem, W. E. Price, M. Elimelech, Comparison of the removal of hydrophobic trace organic contaminants by forward osmosis and reverse osmosis., Water research 46 (8) (2012) 2683–2692. doi:10.1016/j.watres.2012.02.023.

[2] N. T. Hancock, T. Y. Cath, Solute coupled diffusion in osmotically driven membrane processes., Environmental science & technology 43 (17) (2009) 6769–75.

[3] N. T. Hancock, W. a. Phillip, M. Elimelech, T. Y. Cath, Bidirectional permeation of electrolytes in osmotically driven membrane processes., Environmental science & technology 45 (24) (2011) 10642–51. doi:10.1021/es202608y.

[4] G. J. Irvine, S. Rajesh, M. Georgiadis, W. A. Phillip, Ion selective permeation through cellulose acetate membranes in forward osmosis., Environmental science & technology 47 (23) (2013) 13745–53. doi:10.1021/es403581t.

[5] X. Lu, C. Boo, M. Elimelech, Bidirectional Diffusion of Ammonium and Sodium Cations in Forward Osmosis: Role of Membrane Active Layer Surface Chemistry and Charge, Environmental Science & Technology 48 (2014) 14369–14376.

[6] J. T. Arena, M. Chwatko, H. A. Robillard, J. R. McCutcheon, pH Sensitivity of Ion Exchange through a Thin Film Composite Membrane in Forward Osmosis, Environmental Science and Technology Letters 2 (7) (2015) 177–182. doi:10.1021/acs.estlett.5b00138.

[7] W. Cheng, X. Lu, Y. Yang, J. Jiang, J. Ma, Influence of composition and concentration of saline water on cation exchange behavior in forward osmosis desalination, Water Research 137 (2018) 9–17. doi:10.1016/j.watres.2018.02.048.

[8] A. K. D'Haese, I. De Leersnyder, P. Vermeir, A. R. Verliefde, On negative rejection of uncharged organic solutes in forward osmosis, Journal of Membrane Science 548 (May 2017) (2018) 22–31. doi:10.1016/j.memsci.2017.11.002.

[9] F.-x. Kong, H.-w. Yang, Y.-q. Wu, X.-m. Wang, Y. F. Xie, Rejection of pharmaceuticals during forward osmosis and prediction by using the solution–diffusion model, Journal of Membrane Science 476 (2015) 410–420. doi:10.1016/j.memsci.2014.11.026.

[10] M. Sauchelli, G. Pellegrino, A. D'Haese, I. Rodríguez-Roda, W. Gernjak, Transport of trace organic compounds through novel forward osmosis membranes: Role of membrane properties and the draw solution, Water Research 141 (2018) 65–73. doi:10.1016/j.watres.2018.05.003.

[11] F. A. Long, W. F. McDevit, Activity Coefficients of Nonelectrolyte Solutes in Aqueous Salt Solutions., Chemical reviews 51 (1) (1952) 119–169.

[12] N. Ni, S. H. Yalkowsky, Prediction of Setschenow constants, International journal of pharmaceutics 254 (December 2002) (2003) 167–172. doi:10.1016/S0378-5173(03)00008-5.

[13] G. Bargeman, J. M. Vollenbroek, J. Straatsma, C. G. P. H. Schroën, R. M. Boom, Nanofiltration of multi-component feeds. Interactions between neutral and charged components and their effect on retention, Journal of Membrane Science 247 (1-2) (2005) 11–20. doi:10.1016/j.memsci.2004.05.022.

[14] S. Bouranene, A. Szymczyk, P. Fievet, A. Vidonne, Influence of inorganic electrolytes on the retention of polyethyleneglycol by a nanofiltration ceramic membrane, Journal of Membrane Science 290 (2007) 216–221. doi:10.1016/j.desal.2007.10.090.

[15] M. Nilsson, G. Tr??g??rdh, K. ??stergren, The influence of pH, salt and temperature on nanofiltration performance, Journal of Membrane Science 312 (1-2) (2008) 97–106. doi:10.1016/j.memsci.2007.12.059.

[16] J. Luo, Y. Wan, Effect of highly concentrated salt on retention of organic solutes by nanofiltration polymeric membranes, Journal of Membrane Science 372 (1-2) (2011) 145–153. doi:10.1016/j.memsci.2011.01.066.

[17] H. J. C. Berendsen, Transport Properties Computed by Linear Response through Weak Coupling to a Bath (1991). doi:10.1007/978-94-011-3546-7_7.

[18] R. Krishna, J. Wesselingh, The Maxwell-Stefan approach to mass transfer, Chemical Engineering Science 52 (6) (1997) 861–911. doi:10.1016/S0009-2509(96)00458-7.

[19] F. Fornasiero, J. M. Prausnitz, C. J. Radke, Multicomponent Diffusion in Highly Asymmetric Systems. An Extended Maxwell - Stefan Model for Starkly Different-Sized, Segment-Accessible Chain Molecules, Macromolecules 38 (2005) 1364–1370. doi:10.1021/ma040133v.

[20] C. P. J. Ribeiro, B. D. Freeman, D. R. Paul, Modeling of multicomponent mass transfer across polymer films using a thermodynamically consistent formulation of the Maxwell-Stefan equations in terms of volume fractions, Polymer 52 (18) (2011) 3970–3983. doi:10.1016/j.polymer.2011.06.042.

[21] R. Krishna, Describing mixture permeation across polymeric membranes by a combination of Maxwell-Stefan and Flory-Huggins models, Polymer 103 (2016) 124–131. doi:10.1016/j.polymer.2016.09.051.

[22] I. M. Van De Ven-Lucassen, T. J. Vlugt Antonius, J. J. Van Der Zanden, T. J. Kerkhof, Using molecular dynamics to obtain Maxwell-Stefan diffusion coefficients in liquid systems, Molecular Physics 94 (3) (1998) 495–503. doi:10.1080/002689798168006.

[23] B. R. Staples, R. L. Nuttall, The activity and osmotic coefficients of aqueous calcium chloride at 298.15 K, Journal of Physical and Chemical Reference Data 6 (2) (1977) 385–408. doi:10.1063/1.555551.

[24] D. Paul, Reformulation of the solution-diffusion theory of reverse osmosis, Journal of Membrane Science 241 (2) (2004) 371–386. doi:10.1016/j.memsci.2004.05.026.

[25] J. G. Wijmans, R. W. Baker, The solution-diffusion model: a review, Journal of Membrane Science 107 (1-2) (1995) 1–21. doi:10.1016/0376-7388(95)00102-I.

[26] A. Tiraferri, N. Y. Yip, A. P. Straub, S. Romero-Vargas Castrillon, M. Elimelech, A method for the simultaneous determination of transport and structural parameters of forward osmosis membranes, Journal of Membrane Science 444 (2013) 523–538. doi:10.1016/j.memsci.2013.05.023.

[27] A. E. Yaroshchuk, Y. P. Boiko, A. L. Makovetskiy, Filtration potential across membranes containing selective layers, Langmuir 18 (13) (2002) 5154–5162. doi:10.1021/la025503s.

[28] M. Sbaï, P. Fievet, A. Szymczyk, B. Aoubiza, A. Vidonne, A. Foissy, Streaming potential, electroviscous effect, pore conductivity and membrane potential for the determination of the surface potential of a ceramic ultrafiltration membrane, Journal of Membrane Science 215 (1-2) (2003) 1–9. doi:10.1016/S0376-7388(02)00553-7.

[29] L. Bian, Y. Fang, X. Wang, Experimental investigation into the transmembrane electrical potential of the forward osmosis membrane process in electrolyte solutions., Membranes 4 (2) (2014) 275–86. doi:10.3390/membranes4020275.

[30] V. Freger, Swelling and Morphology of the Skin Layer of Polyamide Composite Membranes : An Atomic Force Microscopy Study, Environmental science {{}{&}{}} technology 38 (11) (2004) 3168–3175.

[31] G. M. Geise, H. B. Park, A. C. Sagle, B. D. Freeman, J. E. McGrath, Water permeability and water/salt selectivity tradeoff in polymers for desalination, Journal of Membrane Science 369 (1-2) (2011) 130–138. doi:10.1016/j.memsci.2010.11.054.

[32] G. M. Geise, D. R. Paul, B. D. Freeman, Fundamental water and salt transport properties of polymeric materials, Progress in Polymer Science 39 (1) (2014) 1–42. doi:10.1016/j.progpolymsci.2013.07.001.

[33] S. Zhang, R. Zhang, Y. C. Jean, D. R. Paul, T. S. Chung, Cellulose esters for forward osmosis: Characterization of water and salt transport properties and free volume, Polymer 53 (13) (2012) 2664–2672. doi:10.1016/j.polymer.2012.04.024.

[34] W. J. Hamer, Y.-C. Wu, Osmotic Coefficients and Mean Activity Coefficients of Uni-univalent Electrolytes in Water at 25C, Journal of Physical and Chemical Reference Data 1 (4) (1972) 1047. doi:10.1063/1.3253108.

[35] I. M. Sobol, Sensitivity analysis for nonlinear mathematical models, Mathematical Modelling Computational Experiments 1 (4) (1993) 407–414. doi:10.18287/0134-2452-2015-39-4-459-461.

[36] A. Saltelli, T. Homma, Importance measures in global sensitivity analysis of model output, Reliab. Eng. Sys. Safety 52 (1) (1996) 1–17.

[37] I. M. Sobol, Global sensitivity indices for nonlinear mathematical models. Review, Mathematics and Computers in Simulation 55 (2001) 271–280.

[38] D. G. Leaist, Determination of ternary diffusion coefficients by the Taylor dispersion method, Journal of Physical Chemistry 94 (12) (1990) 5180–5183. doi:10.1021/j100375a075.

[39] L. Ma, L. Gutierrez, M. Vanoppen, D. N. Lorenz, C. Aubry, A. Verliefde, Transport of uncharged organics in ion-exchange membranes: experimental validation of the solution-diffusion model, Journal of Membrane Science 564 (July) (2018) 773–781. doi:10.1016/j.memsci.2018.07.029.

[40] A. D'Haese, M. M. Motsa, P. Van der Meeren, A. R. Verliefde, A refined draw solute flux model in forward osmosis: Theoretical considerations and experimental validation, Journal of Membrane Science 522 (2017) 316–331. doi:10.1016/j.memsci.2016.08.053.

[41] J. Bearman, On the molecular basis of some theories of diffusion, Journal of Physical Chemistry 65 (11) (1961) 1961–1968.

[42] A. Kubaczka, Prediction of Maxwell-Stefan diffusion coefficients in polymer-multicomponent fluid systems, Journal of Membrane Science 470 (2014) 389–398. doi:10.1016/j.memsci.2014.06.055.

[43] E. Dražević, K. Košutić, V. Kolev, V. Freger, Does hindered transport theory apply to desalination membranes?, Environmental Science and Technology 48 (19) (2014) 11471–11478. doi:10.1021/es502085p.

[44] M. T. M. Pendergast, J. M. Nygaard, A. K. Ghosh, E. M. Hoek, Using nanocomposite materials technology to understand and control reverse osmosis membrane compaction, Desalination 261 (3) (2010) 255–263. doi:10.1016/j.desal.2010.06.008.

[45] R. Epsztein, E. Shaulsky, M. Qin, M. Elimelech, Activation behavior for ion permeation in ion-exchange membranes: Role of ion dehydration in selective transport, Journal of Membrane Science 580 (January) (2019) 316–326. doi:10.1016/j.memsci.2019.02.009.

Highlights of "Interactions between feed solutes and inorganic electrolytic draw solutes in forward osmosis"

Arnout K.H. D'Haese

June 18, 2019

- A comprehensive FO transport model based on Maxwell-Stefan theory is presented
- Active layer feed solute transport is determined by membrane interactions only
- Support layer feed solute transport is coupled to both water and draw solute fluxes
- Electromigration is an important driving force for ionic feed solute transport
- Salting out can increase organic feed solute rejection in FO

Declaration of interests

☒ The authors declare that they have no known competing financial interests or personal relationships that could have appeared to influence the work reported in this paper.

☐The authors declare the following financial interests/personal relationships which may be considered as potential competing interests: